

# Strategy for the inversion of Hinode spectropolarimetric measurements in the quiet Sun

David OROZCO SUÁREZ<sup>1</sup>, Luis R. BELLOT RUBIO<sup>1</sup>, Jose Carlos DEL TORO INIESTA<sup>1</sup>, Saku TSUNETA<sup>2</sup>, Bruce W. LITES<sup>3</sup>, Kiyoshi ICHIMOTO<sup>2</sup>, Yukio KATSUKAWA<sup>2</sup>, Shin'ichi NAGATA<sup>4</sup>, Toshifumi SHIMIZU<sup>5</sup>, Richard A. SHINE<sup>6</sup>, Yoshinori SUEMATSU<sup>2</sup>, Theodore D. TARBELL<sup>6</sup>, and Alan M. TITLE<sup>6</sup>

<sup>1</sup>*Instituto de Astrofísica de Andalucía (CSIC), Apdo. de Correos 3004, 18080 Granada, Spain; orozco@iaa.es*

<sup>2</sup>*National Astronomical Observatory of Japan, 2-21-1 Osawa, Mitaka, Tokyo 181-8588, Japan*

<sup>3</sup>*High Altitude Observatory, National Center for Atmospheric Research, P.O. Box 3000, Boulder, CO 80307, USA*

<sup>4</sup>*Hida Observatory, Kyoto University, Kamitakara, Gifu 506-1314, Japan*

<sup>5</sup>*Institute of Space and Astronautical Science, Japan Aerospace Exploration Agency, Tokyo, Japan*

<sup>6</sup>*Lockheed Martin Solar and Astrophysics Laboratory, B/252, 3251 Hanover St., Palo Alto, CA 94304, USA*

(Received 2007 July 15; accepted 2007 September 13)

## Abstract

In this paper we propose an inversion strategy for the analysis of spectropolarimetric measurements taken by *Hinode* in the quiet Sun. The spectropolarimeter of the Solar Optical Telescope aboard *Hinode* records the Stokes spectra of the Fe I line pair at 630.2 nm with unprecedented angular resolution, high spectral resolution, and high sensitivity. We discuss the need to consider a *local* stray-light contamination to account for the effects of telescope diffraction. The strategy is applied to observations of a wide quiet Sun area at disk center. Using these data we examine the influence of noise and initial guess models in the inversion results. Our analysis yields the distributions of magnetic field strengths and stray-light factors. They show that quiet Sun internetwork regions consist mainly of hG fields with stray-light contaminations of about 0.8.

**Key words:** Sun: magnetic fields – Sun: photosphere – Instrumentation: high angular resolution

## 1. Introduction

*Hinode* (Kosugi et al. 2007) is the first solar satellite carrying a full vector spectropolarimeter (SP; Lites et al. 2001). Since its launch in September 2006, the instrument has been taking high-precision, high-angular resolution measurements of the Fe I lines at 630.2 nm. With a pixel size of  $0''.16$ , the angular resolution achieved by the SP is about  $0''.32$ , very close to the diffraction limit of the *Hinode* 0.5m Solar Optical Telescope (Suematsu et al. 2007; Tarbell et al. 2007; Tsuneta et al. 2007). Such an unprecedented spatial resolution opens exciting possibilities for the analysis of the weak magnetic signals observed in the quiet Sun. It should permit, for instance, a better isolation of the magnetic elements that form the quiet photosphere, provided they are not organized on scales much smaller than  $0''.1$ . The increased spatial resolution may result in significantly larger polarization signals than those recorded on the ground. This would minimize the influence of noise, which has long been recognized as one of the main problems in the study of quiet Sun magnetic fields.

The availability of very high angular resolution observations, virtually free from seeing effects, is also important for other reasons. Since the light entering one pixel comes from a much smaller region of the solar surface, the effect of different atmospheres contributing to the intensity and polarization profiles is decreased. This should facilitate the interpretation of the measurements, as relatively sim-

ple one-component atmospheres may be sufficient to explain the observations. Stokes inversions of ground-based data are usually performed in terms of two-component atmospheres because the intensity and polarization profiles are not compatible with the signals emerging from a homogeneous magnetic atmosphere, due to the relatively modest angular resolution attained.

Both the smaller influence of noise and the possibility of using simple model atmospheres make high resolution measurements ideal to study the magnetism of the quiet solar photosphere. Space-borne observations may also shed light on the capabilities of the visible Fe I lines at 630.2 nm, which have recently been put into question by Martínez González et al. (2006a,b). First attempts to clarify the diagnostic potential of these lines at high spatial resolution have been carried out by Khomenko et al. (2007a,b). In a previous paper (Orozco Suárez et al. 2007), we have investigated the same problem using radiative magnetoconvection calculations. We simulated *Hinode*/SP measurements and inverted them in terms of one-component atmospheres accounting for stray/scattered light. The main result of those tests is that Milne-Eddington (ME) inversions of high-angular resolution Fe I 630.2 nm measurements do recover the actual field strengths present in the simulation snapshots. We therefore suggested that the spectropolarimeter aboard *Hinode* would be appropriate for quiet Sun magnetism studies.

Here we investigate in detail critical aspects of the in-

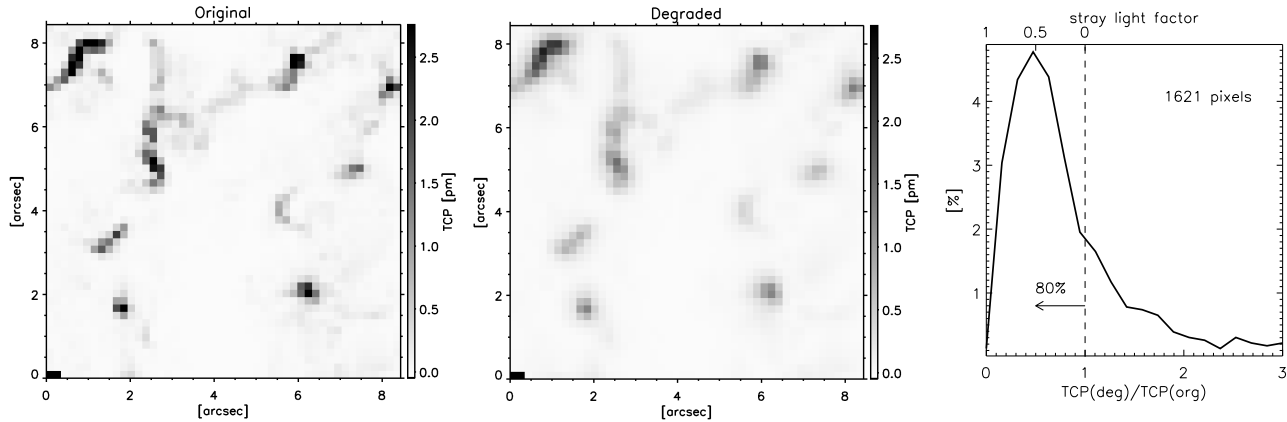


**Fig. 1.** Total circular polarization signals,  $TCP = \int |V| d\lambda / I_c$ , in the original (*left*) and degraded (*middle*) snapshots. *Right:* Histogram representing the ratio of total circular polarization signal in the degraded image with respect to that in the original image. The upper *x*-axis indicates the equivalent stray-light contamination factor.

version, such as the meaning of the stray/scattered light contamination used by Orozco Suárez et al. (2007) and the influence of noise. We also apply our inversion strategy to *Hinode*/SP measurements of quiet Sun areas at disk center. Our preliminary results suggest that most of the magnetic fields present in internetwork regions are weak, in good qualitative agreement with the picture derived from ground-based, near-infrared observations.

## 2. Inversion strategy

The SP aboard *Hinode* was designed to perform high sensitivity polarization measurements with an unprecedented spatial resolution of  $0''.32$  and high spectral resolution. These observations make it possible to derive the magnetic and kinematic properties of the solar photosphere. The simplest way to extract quantitative information from the observations is to use a least-squared inversion technique based on ME atmospheres. In Orozco Suárez et al. (2007) we demonstrated that the field strengths derived from ME inversions of the Fe I 630.2 nm lines observed at  $0''.32$  correspond, on average, to the actual fields present at optical depth  $\log \tau_5 \sim -2$ . In that paper we simulated *Hinode*/SP observations with the help of radiative magnetoconvection simulations. The simulated spectra were inverted in terms of simple one-component model atmospheres filling the resolution element. The use of a *local* stray/scattered light profile was found to be essential for retrieving correct magnetic field strengths.

To understand the meaning of this stray/scattered light contribution, we resort again to the MHD simulations of Vögler et al. (2005) and Schüssler et al. (2003). More specifically, we consider a simulation snapshot with unsigned average flux of  $10 \text{ Mx cm}^{-2}$ . We are certainly aware of the limitations of current MHD calculations, but the fact is that they represent the best option to simulate high resolution observations of quiet Sun internetwork (IN) areas. We have spatially degraded the polarization maps (at each wavelength and each Stokes parameter) by tele-

scope diffraction and rebinned them to match the CCD pixel size of the SP (see Orozco Suárez et al. 2007 for details). In Fig. 1 we represent the total circular polarization,  $\int |V| d\lambda / I_c$ , for the original and degraded data. The visible pixilation corresponds to a size of  $0''.16$ . There are two main effects caused by degradation: first, the polarization signals appear to be "blurred" in the degraded image and, secondly, there is a substantial loss of contrast caused by a weakening of the polarization signals.

To evaluate more quantitatively the effects of telescope diffraction, the right panel of Fig. 1 displays the ratio of total circular polarization signal in the degraded snapshot with respect to that in the original snapshot. Only pixels whose Stokes  $Q$ ,  $U$ , or  $V$  amplitudes remain larger than  $4.5 \times 10^{-3} I_c$  after degradation and binning to the SP pixel size are considered here. This leaves us with 1621 pixels. The histogram indicates that the circular polarization is smaller in the degraded image: 80% of the pixels show weaker signals. The decrease in polarization signal is not due to cancellation of opposite polarity fluxes (since mixed polarities are not present in the snapshot at very small spatial scales), but is truly the result of diffraction. If one does not account for this reduction, the inversion would systematically fail, giving too small field strengths where the magnetic field is intrinsically weak. For this reason it is important to use a stray/scattered light contamination factor. Since telescope diffraction mixes light from nearby pixels, not from pixels far away, a local stray-light profile must be considered.

Admittedly, our treatment of telescope diffraction is simplistic because we use an *unpolarized* stray-light contamination, while it is clear that diffraction also mixes the polarization signals. As a result, pixels which show larger polarization signals after degradation cannot be dealt with properly. However, it represents a significant improvement over conventional treatments in which a single global stray-light profile is employed to invert the observed region. This is illustrated in Fig. 2, where we show an example of simulated *Hinode*/SP observations inverted

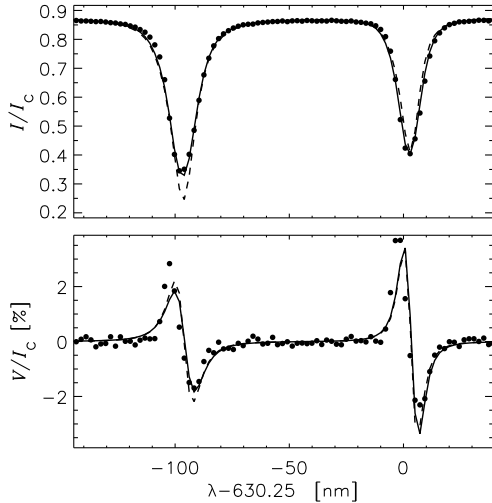


**Fig. 2.** Observed (*dots*) and best-fit Stokes  $I$  and  $V$  profiles from simulated *Hinode*/SP observations using a global (*dashed*) and a local (*solid*) stray-light profile contamination in the inversion.

with a global and a local stray-light profile. The best fit using a global stray-light contamination cannot simultaneously explain the intensity and polarization spectra because the stray-light profile has a different shape than that needed to account for the observed Stokes  $I$  profile. The problem disappears when a local stray-light profile is used, which also improves the determination of the intrinsic field strength. In conclusion, even if our treatment is simple, the results of Orozco Suárez et al. (2007) show that it does work.

To analyze *Hinode*/SP observations of quiet sun regions we propose the approach described by Orozco Suárez et al. (2007), i.e., a least-squares inversion technique based on ME atmospheres with simple one-component models and a local stray-light contamination factor. As a first approximation, we suggest to evaluate the stray-light profile individually for each pixel as the average of the Stokes  $I$  profiles observed in a box  $1''$ -wide centered on the pixel. The inversion can be performed with only 10 free parameters: the three components of the magnetic field (strength  $B$ , inclination  $\gamma$ , and azimuth  $\chi$ ), the line-of-sight velocity ( $v_{\text{LOS}}$ ), the two parameters describing the linear dependence of the source function on optical depth ( $S_0$  and  $S_1$ ), the line strength ( $\eta_0$ ), the Doppler width ( $\Delta\lambda_D$ ), the damping parameter ( $a$ ), and the stray-light factor ( $\alpha$ ). No broadening by macroturbulence needs to be considered. Broadening by microturbulent velocities should effectively be accounted for by the Doppler width parameter.

### 3. Observations

We put the inversion strategy into practice by analyzing a quiet solar region of  $327'' \times 164''$  observed with the *Hinode* SP at disk center on March 10, 2007. This scan has also been studied by Lites et al. (2007a,b). The spectrograph slit, of width  $0.16''$ , was moved across the solar

surface in steps of  $0.1476''$  to measure the four Stokes profiles of the Fe I lines at 630.2 nm. The SP samples the profiles with  $2.15 \text{ pm pixel}^{-1}$ . The integration time per slit position was 4.8 s, so completion of the map took about 3 hours. The data have been corrected for various instrumental effects and calibrated as described by Lites et al. (2007c). After the reduction process, the noise levels turn out to be  $1.1 \times 10^{-3} I_c$  in Stokes  $V$  and  $1.2 \times 10^{-3} I_c$  in Stokes  $Q$  and  $U$ , as measured in continuum wavelength regions.

Figure 3 shows continuum intensities and total polarization signals,  $\int (Q^2 + U^2 + V^2)^{1/2} d\lambda / I_c$ , for a small subfield of  $73.8'' \times 39.6''$ . The high contrast of the granulation in the continuum intensity map testifies to the quality of the observations. In the polarization map one can easily identify a super-granular cell outlined by the network. The stronger polarization signals correspond to areas where the granulation is distorted. Note that the gray scale for the total polarization map has been clipped at 1.5 pm. Within the cell interior, i.e., the internetwork, we find weaker magnetic signals. The nature of these IN fields is a controversial topic.

### 4. Inversion results

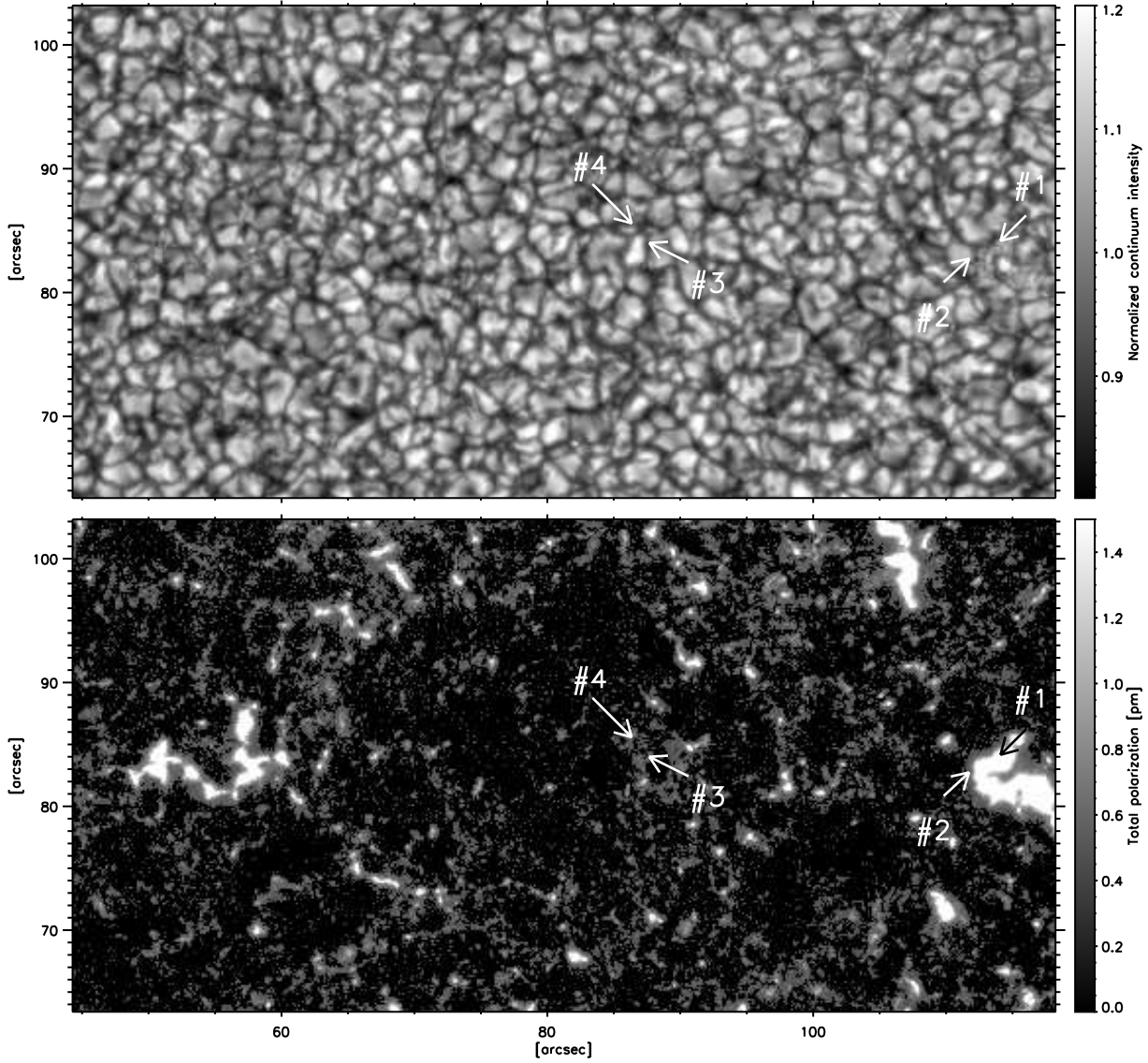
The Stokes spectra measured by the *Hinode* SP have been inverted using the MILOS<sup>1</sup> code (Orozco Suárez & del Toro Iniesta 2007). Figure 4 displays sample fits for individual pixels belonging to the network. Pixel #1 (*left*) represents a typical network element at the center of strong flux concentrations, whereas pixel #2 (*right*) comes from the edge of a network patch. For both pixels the fits to Stokes  $V$  are not very successful due to the asymmetries of the profiles. Note that ME profiles are *symmetric* by definition. At the edges of network patches one can see that the Stokes  $V$  amplitude of Fe I 630.15 nm is usually larger than that of the 630.25 nm line. The inversion returns a field strength of 1334 G, a field inclination of  $19^\circ$ , and a field azimuth of  $136^\circ$ , with a stray light factor of 61%, for pixel #1, and a field strength, inclination, and azimuth of 237 G,  $69^\circ$ , and  $160^\circ$  with a stray light factor of 71%, for pixel #2.

Figure 5 displays sample profiles as well, but in this case for two pixels belonging to the IN. The observed Stokes  $V$  amplitudes exceed  $\sim 10$  and  $\sim 13$  times the noise level, respectively. In contrast to the profiles coming from the network, Fe I 630.15 nm shows significantly smaller Stokes  $V$  amplitudes than Fe I 630.25 nm, suggesting weak fields. The inversion indeed confirms this point, retrieving field strengths, inclinations and azimuths of 247 G,  $141^\circ$  and  $248^\circ$  for pixel #3 (*left*) and 380 G,  $115^\circ$  and  $164^\circ$  for pixel #4 (*right*).<sup>2</sup> The stray light contamination factor in the two cases is 88% and 85%, respectively.

Overall, the quality of the fits is remarkably good keeping in mind the limitations of the ME approximation and

<sup>1</sup> MILne-Eddington inversion of pOLarized Spectra

<sup>2</sup> The azimuth values are less reliable when the Stokes  $U$  and  $Q$  signals approach the noise level, as in pixel #2 (Fig. 4) or pixel #3 (Fig. 5).



**Fig. 3.** Subfield of  $73.8'' \times 39.6''$  showing continuum intensities (*top*) and total polarization signals,  $\int(Q^2 + U^2 + V^2)^{1/2} d\lambda/I_c$ , (*middle*). The gray scale for the total polarization saturates at 1.5 pm. The granulation contrast is 7.44%. Four pixel positions are indicated with numbers. Pixels #1 and #2 belong to the network, while #3 and #4 are representative of IN regions.

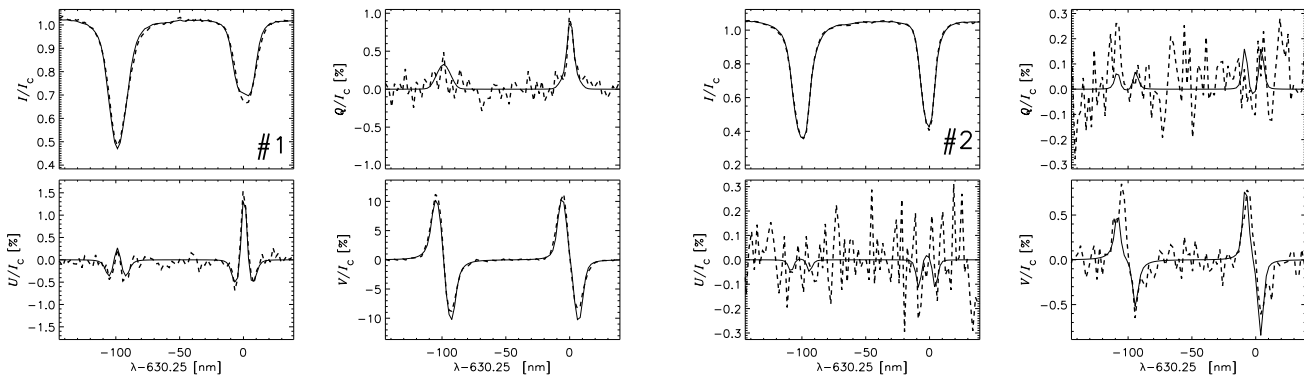


**Fig. 4.** Observed (*dashed*) and best-fit (*solid*) Stokes profiles emerging from network pixels #1 (*left*) and #2 (*right*). The field strengths and the stray-light factors retrieved from the inversion are 1334 and 237 G, and 61 and 71%, respectively.

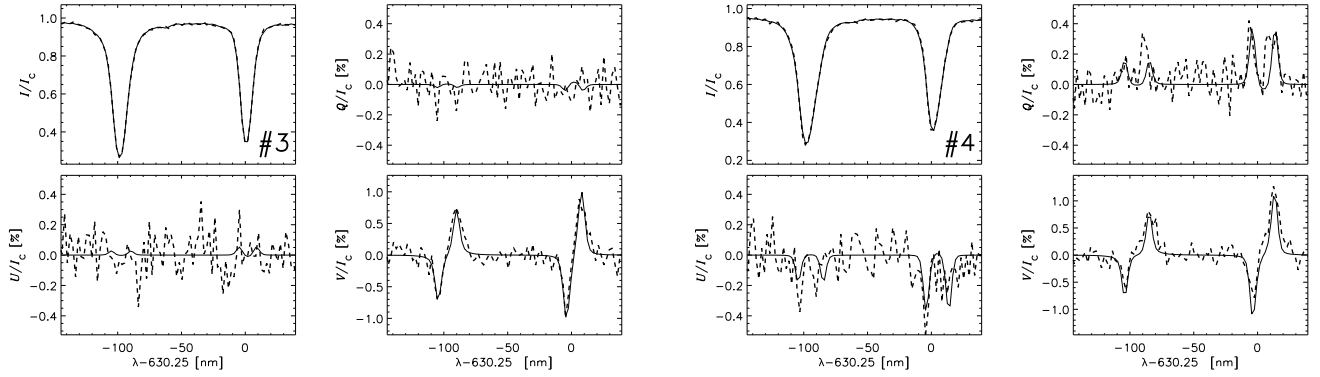


**Fig. 5.** Observed (*dashed*) and best-fit (*solid*) Stokes profiles emerging from the internetwork. The field strength and the stray-light factor are 247 and 380 G for pixel #3 (*left*) and 88 and 85% for pixel #4 (*right*), respectively.

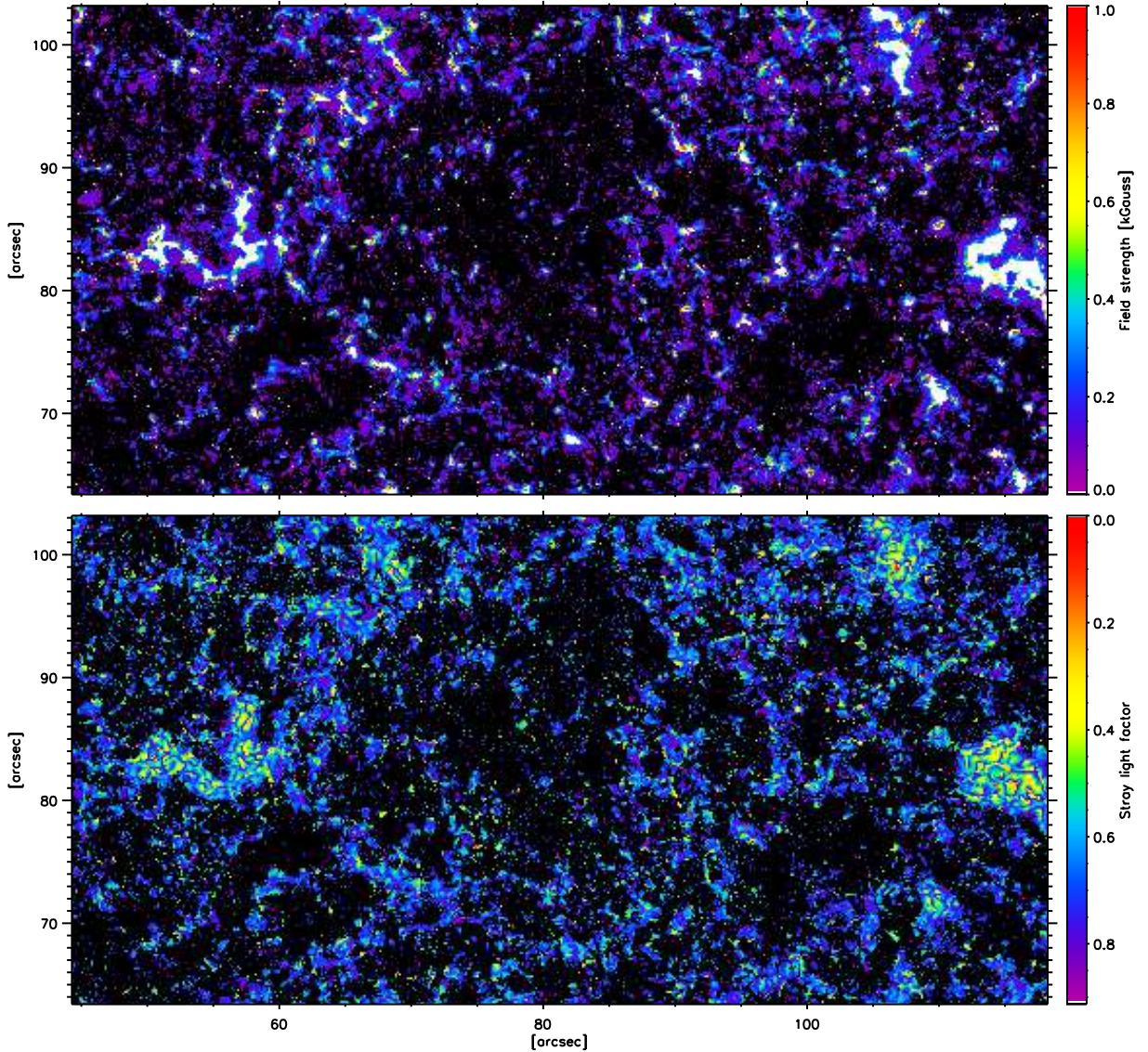


**Fig. 6.** Same as Fig. 3 but for the magnetic field strengths (*top*) and stray-light factors (*bottom*) inferred from the inversion. As in Fig. 3, network and internetwork areas can easily be identified. Black areas correspond to non-inverted pixels. The field strength color bar is clipped at 1000 G (*white*).

the fact that only one-component atmospheres are used.

Maps of the retrieved field strengths and stray light factors are shown in Fig. 6. In both maps, black regions represent pixels whose Stokes  $Q$ ,  $U$  and  $V$  signals are smaller than 4.5 times the noise level. These pixels have not been inverted to avoid unreliable results. As in the TCP map, two different regions can be identified: the network, characterized by strong fields (above 1 kG), and the IN, with much weaker fields and slightly larger stray-light factors.

Figure 7 displays the distribution of field strengths and stray-light factors, for the full FOV and for IN regions, given as probability density functions (PDFs). IN areas have been selected manually in the interior of supergranular cells, avoiding the strong flux concentrations of the network. The PDF of the field strength in the full FOV peaks at about 90 G and then decreases rapidly toward stronger fields. There are very few kG fields in this quiet Sun region. The PDF of the stray-light factors shows that most pixels require large values of stray-light contamination, with a maximum at around 0.8.

According to our discussion in Sect. 2, we interpret the stray-light contamination as a degradation of the polarization signals due to diffraction, but it might also represent magnetic filling factors smaller than 1. An effective filling factor can be computed as  $f = 1 - \alpha$ . If one accepts this alternative interpretation, then the fractional area of the resolution element occupied by magnetic fields would be small, showing a peak at  $f \sim 0.2$ . We note, however, that the histogram of polarization signal ratios presented in Fig. 1 has a maximum at around 0.5, so the stray-light factors of  $\sim 0.8$  derived from the inversion might actually represent two different effects: telescope diffraction ( $\sim 50\%$ ) and a real filling factor due to still insufficient angular resolution ( $\sim 30\%$ ). In other words, the stray-light contaminations required to explain the measurements of the *Hinode* SP may imply an average magnetic filling factor (per pixel) of  $f \sim 0.7$  in the quiet Sun. Given that different interpretations are possible, further work should be carried out to investigate the exact meaning of the stray-light factors inferred from ME inversions of *Hinode*/SP measurements.

## 5. Influence of noise

The polarization signals in the internetwork are typically smaller than those in active regions. As a result, they are more affected by noise. This may make the determination of vector magnetic fields less reliable. To minimize the influence of noise we have analyzed only Stokes profiles whose polarization signals exceed a given threshold above the noise level  $\sigma$ . The inversions presented so far correspond to pixels whose  $Q$ ,  $U$  or  $V$  signals are larger than  $4.5\sigma$ . This should increase the robustness of the results because we do not include too noise profiles in the analysis. Our experience with simulations and real observations tells us that ME inversions provide reliable results in the quiet Sun under these conditions.

To evaluate the effect of noise in more detail we have calculated the field strength PDF of IN regions for three

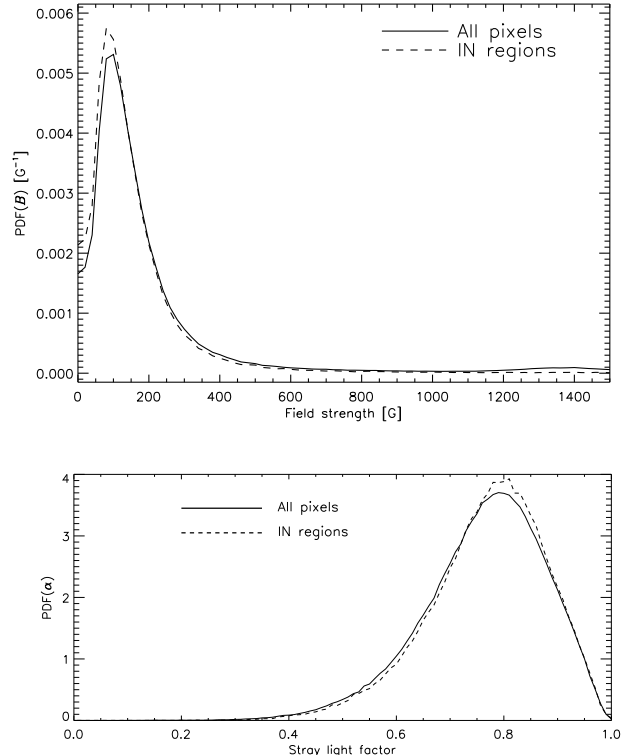


**Fig. 7.** *Top:* Magnetic field strength PDF for all pixels in the FOV and IN regions. *Bottom:* PDF of the stray-light factor. *Solid and dashed lines* represent the full FOV and IN regions, respectively.

different thresholds: 5, 7.5, and  $10\sigma$ . Figure 8 displays the results. As the threshold level increases, the peak of the PDF decreases in amplitude, shifts toward stronger fields, and becomes broader. Thus, the larger the threshold, the smaller the percentage of weak fields detected. Since weak fields are usually associated with weak polarization signals for fully resolved magnetic structures, this is exactly what one would expect just because the weak polarization signals are excluded from the analysis. The important result is that, independently of the polarization threshold used, the amount of strong fields remains unchanged. Even for very high polarization thresholds, the field strength PDFs are dominated by weak fields, so they cannot be the result of noise in the profiles.

Further support to our claim that noise is not producing an artificial excess of weak fields comes from the inversion of the deep mode observations analyzed by Lites et al. (2007a,b). The deep-mode data are single-slit position measurements with effective exposure times of 67.2 s, which lowers the rms noise in Stokes  $Q$ ,  $U$  and  $V$  down to about  $3 \times 10^{-4} I_c$  without compromising the spatial resolution. These observations have a S/N about 3.7 times larger than that of the measurements considered in this paper. A polarization threshold of 4.5 times the new noise level is equivalent to a threshold of 1.2 times the noise level of our observations. When we invert the deep-mode observations with the same code and same free parameters,

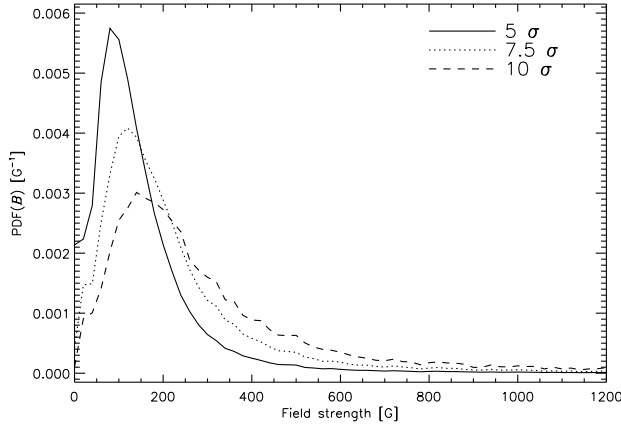


**Fig. 8.** Magnetic field strength probability density function for IN regions. The different line styles stand for different threshold levels in the analysis. Pixels whose Stokes  $Q$ ,  $U$  or  $V$  amplitudes do not exceed these levels are rejected.

we get PDFs for the field strength and stray-light factor that are nearly the same as those presented in Fig. 7.

## 6. Influence of the initial guess model

Different initial guess models may lead to different results, which has raised concerns about the uniqueness of the model atmospheres derived from quiet Sun inversions of Fe I 630.15 and 630.25 nm (Martínez González et al. 2006a,b). The MILOS code determines a total of ten free parameters in a maximum number of 300 iterations. We have employed the same initial guess model for all the inversions:  $S_0 = 0.02$ ,  $S_1 = 1$ ,  $\eta_0 = 7.2$ ,  $a = 0.78$ ,  $\Delta\lambda_D = 29$  mÅ,  $v_{LOS} = 0.1$  km/s,  $B = 100$  G,  $\gamma = 30^\circ$ ,  $\chi = 30^\circ$ , and  $\alpha = 10\%$ . How do the results change when a strong-field rather than a weak-field initialization is used? To investigate this issue we have inverted a small IN area of  $32''2 \times 32''2$  adopting different initialization for the magnetic field strength. In particular we have carried out four inversions with initial field strengths of 100, 500, 1000, and 1500 G. Figure 9 shows a histogram of the differences between the field strengths resulting from the 100 and 1500 G initializations. This plot demonstrates that the solutions do not depend on the initial magnetic field strength.

Another indication that the results are largely independent of the initial guess is provided by the fact that the percentage of pixels which gets substantially better fits is small: only 3.1% for the 500 G initialization, 4.7% for the 1000 G initialization, and 4.3% for the 1500 G initialization. Here, “substantially” better fits mean that the final  $\chi^2$  value is at least 50% smaller than the one obtained with 100 G.

In conclusion, even if there are unavoidable differences between the results of different initializations, their magnitude is so small that the field strength and stray-light distributions remain essentially the same. This is in sharp contrast with the inversions of ground-based measure-

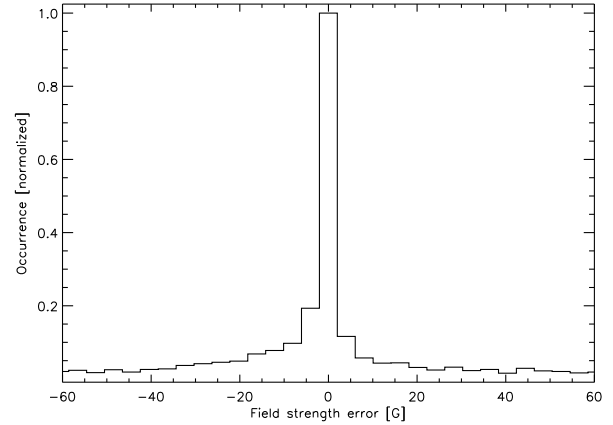


**Fig. 9.** Histogram of the difference between the field strength values inferred with two different initializations, 100 and 1500 G.

ments of the Fe I 630.2 nm lines described by Martínez González et al. (2006a). Additional information on the robustness of inversion codes can be found in e.g. del Toro Iniesta & Ruiz Cobo (1996), Westendorp Plaza et al. (1998), and Bellot Rubio (2006).

## 7. Understanding ME inversions

The tests presented in Sect. 6 demonstrate that ME inversions are capable of disentangling the effects of the various atmospheric parameters. In particular, they successfully distinguish between stray-light factor and magnetic field strength. How is this achieved in the weak field regime that applies in most of the IN pixels?

To answer this question, let us assume that the ME models derived from the inversions of Sect. 4 are the “true” solution. We have repeated the inversion of the profiles observed by *Hinode* fixing the stray-light factor to erroneous values. 101 different stray-light factors, from  $\alpha = 0$  to 1, have been considered. The other parameters for the initial guess model are the same as those described in Sect. 6. In Fig. 10 we represent the  $\chi^2$  values of the 101 fits against the corresponding fixed stray-light factors, for the particular case of pixel #4 in Fig. 5 (the results for other pixels are equivalent). The solid line displays the total  $\chi^2$ , whereas the dotted and dashed lines indicate the  $\chi^2$  values for Stokes  $I$  and  $V$ , respectively. The vertical line represents the “true” solution. Note that  $\chi^2$  is dimensionless and that its absolute value is irrelevant to the inversion code.

This plot gives a clear explanation of what is happening. When the stray-light factor is fixed to erroneous values, the fits worsen and the total  $\chi^2$  increases. The variation of the total merit function is large enough to be detectable by the inversion algorithm. Remarkably, the Stokes  $I$  and  $V$  merit functions behave quite differently. The Stokes  $V$   $\chi^2$  values around  $\alpha = 0.8$  are very similar. This implies that different stray-light contaminations produce equally good fits to Stokes  $V$ . In other words: many compatible

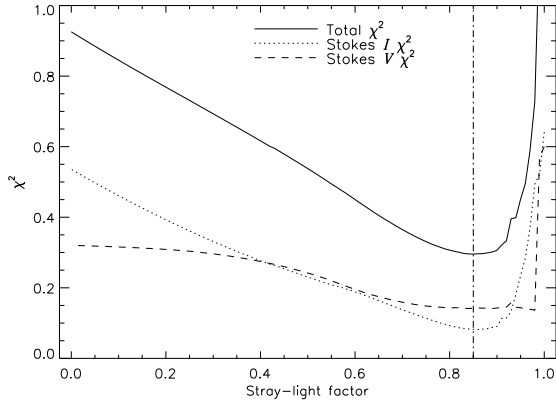


**Fig. 10.**  $\chi^2$  values of the best-fit profiles resulting from the inversion of pixel #4 (as observed by *Hinode*) with fixed, erroneous stray-light factors. The solid, dotted and dashed lines stand for the total, Stokes *I* and *V*  $\chi^2$ , respectively. The vertical line represents the “true” stray-light factor.

solutions, characterized by different stray-light factors and correspondingly different field strengths, exist for Stokes *V*. However, the range of acceptable stray-light contaminations is strongly limited by Stokes *I*. This is reflected in the rapid increase of the Stokes *I* merit function away from the correct stray-light factor. The conclusion is the following: for the most part, the inversion algorithm uses the information encoded in Stokes *I* to determine the stray-light contamination. Thus, the often forgotten Stokes *I* also plays an essential role in the process of finding the absolute minimum of the total merit function.

## 8. Conclusions

In this paper we have proposed a simple Milne-Eddington inversion to interpret the high spatial resolution spectropolarimetric measurements of the quiet Sun performed by *Hinode*. Using magnetoconvection simulations, we have shown that it is important to include a stray light contamination factor in the analysis. The stray light profile should be evaluated locally in order to account for the effects of telescope diffraction.

The inversion strategy has been applied to a quiet Sun raster scan taken with the *Hinode* SP. We have demonstrated that noise does not significantly affect the results of ME inversions, provided a sufficiently large polarization threshold is used to invert the Stokes profiles. A threshold around 4.5 times the noise level seems to yield correct inferences. In addition, we have shown that the results do not depend on the initial magnetic field strength of the model, because the information contained in the Stokes profiles observed at the resolution of *Hinode* is sufficient to disentangle the various model parameters.

The inferred PDFs of the magnetic field strength indicate that internetwork regions are mainly formed by hG field concentrations with large stray light factors. Taking into account the weakening of the polarization signals due to telescope diffraction, these large stray light factors

might also be interpreted as magnetic filling factors of the order of 0.7. The preliminary analysis presented here confirms the picture of weak internetwork fields derived from ground-based measurements in the near infrared (see, e.g., Collados 2001).

*Hinode* is a Japanese mission developed and launched by ISAS/JAXA, with NAOJ as domestic partner and NASA and STFC (UK) as international partners. It is operated by these agencies in co-operation with ESA and NSC (Norway). This work has been partially funded by the Spanish Ministerio de Educación y Ciencia through project ESP2006-13030-C06-02 (including European FEDER funds). The NAOJ *Hinode* Science Center is supported by the Grant-in-Aid for Creative Scientific Research “The Basic Study of Space Weather Prediction” from MEXT, Japan (Head Investigator: K. Shibata), generous donations from Sun Microsystems, and NAOJ internal funding.

## References

- Bellot Rubio, L. R. 2006, *Astronomical Society of the Pacific Conference Series*, 358, 107
- Collados, M. 2001, in: *Advanced Solar Polarimetry – Theory, Observation, and Instrumentation*, ASP Conf. Series, 236, 255
- del Toro Iniesta, J. C., & Ruiz Cobo, B. 1996, *Sol. Phys.*, 164, 169
- Khomenko, E., & Collados, M. 2007a, *Mem. Soc. Astr. Italiana*, 78, 166
- Khomenko, E. & Collados, M. 2007b, *ApJ*, 659, 1726
- Kosugi, T. et al. 2007, *Sol. Phys.*, submitted
- Lites, B.W., Elmore, D. F., & Stander, K.V. 2001, *ASP Conf. Ser.*, 236, 33
- Lites, B.W., et al. 2007a, *PASJ*, submitted
- Lites, B.W., et al. 2007b, *ApJ*, submitted
- Lites, B.W., et al. 2007c, *Sol. Phys.*, in preparation
- Martínez González, M.J., Collados, M., & Ruiz Cobo, B. 2006a, *A&A*, 456, 1159
- Martínez González, M.J., Collados, M., & Ruiz Cobo, B. 2006b, *ASP Conf. Series*, 358, 36
- Orozco Suárez, D., & del Toro Iniesta, J.C. 2007, *A&A*, 462, 1137
- Orozco Suárez, D., Bellot Rubio, L.R. & del Toro Iniesta, J.C. 2007, *ApJ*, 662, L31
- Schüssler, M., Shelyag, S., Berdyugina, S., Vögler, A., & Solanki, S.K. 2003, *ApJ*, 597, L173
- Suematsu, Y., et al. 2007, *Sol. Phys.*, submitted
- Tarbell, T., et al. 2007, *Sol. Phys.*, submitted
- Tsuneta, S., et al. 2007, *Sol. Phys.*, submitted
- Vögler, A., Shelyag, S., Schüssler, M., Cattaneo, F., Emonet, T., & Linde, T. 2005, *A&A*, 429, 335
- Westendorp Plaza, C., del Toro Iniesta, J. C., Ruiz Cobo, B., Martínez Pillet, V., Lites, B. W., & Skumanich, A. 1998, *ApJ*, 494, 453